The Astrophysical Journal, 982:70 (10pp), 2025 April 1 https://doi.org/10.3847/1538-4357/adb8d7

Comparison of HMG and Flat Rotation Velocities Inferred from Galaxy–Galaxy Weak Lensing

Robert Monjo[1,2]
[1] Department of Physics and Mathematics, University of Alcalá, Faculty of Sciences, E-28805, Alcalá de Henares, Madrid, Spain; robert.monjo@uah.es
[2] Department of Math and Computer Science, Saint Louis University, Max Aub Street, 5, E-28003, Madrid, Spain
Received 2024 October 5; revised 2025 February 18; accepted 2025 February 19; published 2025 March 20

Abstract

Despite the success of dark matter models, unresolved issues require exploring alternatives such as modified gravity theories. In this context, we examine the compatibility of the hyperconical modified gravity (HMG) with galaxy rotation curves inferred from weak-lensing data. The research addresses the existing limitations of modified Newtonian dynamics (MOND), which often struggle with universal applicability across different galactic scales. By assuming local validity of general relativity and analyzing recent data on circular velocities from galaxy–galaxy weak lensing, our findings interpret the flat rotation curves as an effect of fictitious acceleration inherited from the cosmic expansion, without invoking dark matter. The results indicate that HMG successfully reproduces flat velocity curves on scales of 1 Mpc slightly better than MOND. Therefore, these observations support HMG as a viable gravitational model, highlighting its potential to account for dynamics on galaxies and other scales. Further research with extensive data sets is required to confirm these preliminary insights.

Unified Astronomy Thesaurus concepts: Weak gravitational lensing (1797); Modified Newtonian dynamics (1069); Spacetime metric (1550); Galaxy dynamics (591)

1. Introduction

The dark matter (DM) paradigm has been remarkably successful in explaining a wide range of astrophysical phenomena, from the rotation curves of galaxies to the large-scale structure of the Universe (D. Clowe et al. 2006; C. Frenk & S. White 2012; J. S. Bullock & M. Boylan-Kolchin 2017). For instance, the Bullet Cluster is often cited as one of the strongest pieces of evidence for DM, as gravitational lensing maps reveal a clear separation between the baryonic mass (hot X-ray gas) and the inferred total mass (from lensing effects), which is difficult to explain in purely baryonic or modified gravity frameworks (D. Clowe et al. 2006). However, several open issues persist. Despite extensive efforts, DM particles have yet to be detected directly (L. Roszkowski et al. 2018). Observational phenomena, such as the mass discrepancy acceleration relation (MDAR) and the baryonic Tully–Fisher relation (BTFR), suggest that our understanding of gravity at galactic scales may be incomplete (S. S. McGaugh et al. 2016). In particular, the BTFR is an empirical MDAR found in galaxy dynamics, which is tightly described as a function of the observed baryonic mass M_b without the need for unobservable matter (S. Trippe 2014; D. Merritt 2017; J. S. Goddy et al. 2023). This law is commonly expressed as follows:

$$M_b = A\, v_{\rm flat}^{\epsilon}, \tag{1}$$

with $\epsilon \approx 4$ for the level of the *flat* velocity curve $v_{\rm flat}$ observed in a galaxy disk (see, e.g., J. S. Goddy et al. 2023). Similarly, it can be also expressed as an MDAR (S. S. McGaugh 2004; A. Di Cintio & F. Lelli 2015),

$$\frac{M_b + M_{\rm CDM}}{M_b} = \frac{v^2}{v_N^2} = C|a_{\rm N}|^{-\beta} = C\left(\frac{r}{v_{\rm N}^2}\right)^{\beta}$$
$$\Rightarrow\ v^4 = C^2 r^{2\beta}\, v_{\rm N}^{4(1-\beta)} \approx C^2 {\rm G} M_b, \tag{2}$$

where $\beta \approx 0.5$, $M_b + M_{\rm CDM}$ is the Newtonian dynamical total mass including cold dark matter (CDM), $C^2{\rm G} \approx: A^{-1}$ is approximately the inverse of the constant used in Equation (1), and the Newtonian acceleration $|a_{\rm N}| = {\rm G}M_b/r = v_{\rm N}^2/r$ is expressed as a function of the Kepler–Newton velocity $v_{\rm N}$ and the radial coordinate r measured from the galaxy center. To explain this phenomenon, some studies suggested that DM presents a stronger coupling to baryons, linking both matter contents by an effective law (L. Blanchet 2007; A. Katz et al. 2016; R. Barkana 2018). However, most observations suggest the need to modify the standard gravity models because the mass discrepancy acceleration (with respect to the expected Newtonian gravity) only occurs where the gravity induced by the visible matter is lower than a typical scale with an almost constant value, which points to a more general problem involving scales rather than a problem involving matter types (S. Trippe 2014; D. Merritt 2017; S. Comerón et al. 2023).

Alternative theories such as the Milgromian dynamics (known as modified Newtonian dynamics; MOND), Moffat modified gravity, and hyperconical modified gravity (HMG) propose modifications to gravity that could potentially eliminate the need for DM (M. Milgrom 1983; J. W. Moffat & V. T. Toth 2009; M. Milgrom 2020; R. Monjo 2023).

MOND was introduced by Milgrom in 1983 as an alternative to DM. MOND modifies Newton's second law for accelerations below a certain threshold a_0, leading to the following

effective gravitational acceleration:

$$a_{\rm MOND} = a_N\,\nu\left(\frac{a_N}{a_0}\right) = \begin{cases} a_N & \text{if } a_N \gg a_0 \\ \sqrt{a_N a_0} & \text{if } a_N \ll a_0 \end{cases}, \quad (3)$$

where $a_0 \approx 1.2 \times 10^{-10}\,\mathrm{m\,s^{-2}}$ is the characteristic acceleration scale, while $\nu(x)$ is an interpolation function that satisfies $\nu(x) = 1$ for $x \gg 1$ and $\nu(x) = 1/\sqrt{x}$ for $x \ll 1$. The best-fitting ν function is (S. S. McGaugh et al. 2016; I. Banik & H. Zhao 2022)

$$\nu(x) = \frac{1}{1 - \exp(-\sqrt{x})}. \quad (4)$$

MOND has been successful in reproducing the flat rotation curves of spiral galaxies without invoking DM (R. H. Sanders 2003; S. S. McGaugh et al. 2007). However, its extension to a relativistic theory still presents some unsolved challenges, in addition to problems at smaller scales (I. Banik & H. Zhao 2022; R. Monjo 2023; I. Banik et al. 2024; S. A. Cookson 2024).

HMG is a more recent proposal that modifies the gravitational potential by restricting general relativity (GR) to be valid only at a local scale over a background hyperconical metric (R. Monjo 2024). HMG is a relativistic theory that reproduces the behavior of MOND with a unique natural transition function ν that addresses the shortcomings of MOND in explaining the radial acceleration relation of galaxy clusters (R. Monjo & I. Banik 2024). Specifically, the HMG transition function depends on the distribution of mass and the geometry of spacetime.

To complete our previous findings, this paper analyzes the HMG modeling for flat rotation curves, inferred from weak lensing, recently published (T. Mistele et al. 2024). To analyze the theoretical circular orbital velocities from weak lensing using a specific Lorentzian metric, the authors widely considered the case of a spherically symmetric metric given by $ds^2 = f(r)c^2dt^2 - g(r)dr^2 - r^2(d\theta^2 + \sin^2\theta\, d\phi^2)$, where $f(r)$ and $g(r)$ are functions of the radial coordinate r (M. Bartelmann & P. Schneider 2001; P. Rodríguez-Gil et al. 2005). The enclosed mass $M(r)$ within a radius r is related to the metric functions $f(r)$ and $g(r)$. For a static and spherically symmetric spacetime, $f(r) = g(r)^{-1} = 1 - 2\Phi/c^2$ imitates the Schwarzschild metric, with gravitational potential at r defined by $\Phi(\boldsymbol{r}) \equiv -G\int \rho(\boldsymbol{r}')/|\boldsymbol{r} - \boldsymbol{r}'|\, dV'$, where $\rho(r')$ is the mass density at a point r' distributed around the volume V', and approaches $\Phi(r) = GM(r)/r$ in the classic spherical limit. In the Newtonian regimen, with weak gravity ($r \gg 2GM/c^2$) and low velocities ($v/c \ll 1$), the function $f(r)$ contributes significantly more than the function $g(r)$ to geodesics (M. Bartelmann & P. Schneider 2001; B. P. Dolan 2023).

As a key in weak-lensing analysis, the surface mass density $\Sigma(R)$ at projected distance R is obtained by projecting the mass density $\rho(r)$ along the line of sight according to $\Sigma(R) = 2\int_0^\infty \rho(\sqrt{R^2 + z^2})\, dz$, and the *convergence* or dimensionless surface mass density is given by $\kappa(R) = \Sigma(R)/\Sigma_{\rm crit}$, where $\Sigma_{\rm crit} = \frac{c^2}{4\pi G} D_s D_d^{-1} D_{ds}^{-1}$ is the critical surface mass density for lensing, while D_s, D_d, and D_{ds} are the angular diameter distances from the observer to the source, from the observer to the lens, and from the lens to the source, respectively (see Figure 1 of I. Banik & H. Zhao 2015). These relationships allow us to derive the mass profile from radial acceleration $a_{\rm obs}(r)$ and subsequently calculate the theoretical circular orbital (square) velocity $v_c^2(r) \coloneqq r\, a_{\rm obs}(r)$, which is critical for understanding the dynamics of galaxies through weak-lensing data (P. Rodríguez-Gil et al. 2005; M. M. Brouwer et al. 2021; T. Mistele et al. 2024).

2. Data and Model

2.1. Inferred Observations

This paper uses the published results of T. Mistele et al. (2024) on the observed circular velocity inferred from weak lensing and classified in four bins of baryonic mass (1.29, 4.57, 9.13, and 19.5 in units of $10^{10}\ M_\odot$). Specifically, we use 20 accurate estimates of the *flat* speed ($v_{\rm flat}$) as a function of the observed mass and distances (Table 1 of T. Mistele et al. 2024). Moreover, our work uses baryonic Tully–Fisher data published in the same paper, distinguishing between ranges of 300 kpc and 1 Mpc, as well as between early-type galaxies (ETGs) and late-type galaxies (LTGs). The results are consistent with F. Lelli et al. (2019).

2.2. Metric Perturbation of HMG

Observed orbital speed data inferred from weak lensing were compared to the values modeled by HMG, for the observed baryonic mass, according to the work developed by R. Monjo (2023) and R. Monjo & I. Banik (2024), which is summarized here. Let g be the background metric of the hyperconical Universe (R. Monjo 2017; R. Monjo & R. Campoamor-Stursberg 2023). The metric g is locally approximately given by

$$g \approx dt^2(1 - kr'^2) - \frac{t^2}{t_0^2}\left(\frac{dr'^2}{1 - kr'^2} + r'^2 d\Sigma^2\right) - \frac{2r't}{t_0^2} dr'dt, \quad (5)$$

where $k = 1/t_0^2$ is the spatial curvature for the current value of the age t of the Universe ($t_0 \equiv 1$), while t/t_0 is a linear scale factor, $r' \ll t_0$ is the comoving distance, and Σ represents the angular coordinates. The shift and lapse terms of Equation (5), produced by the comoving observers, lead in turn to an apparent radial spatial inhomogeneity that is assimilated as a fictitious acceleration with adequate projected coordinates.

The HMG model is based on two key ideas:

1. Any gravitational system of mass $M_{\rm sys}$ generates a perturbation over the diagonal terms of the background metric $g \to \hat{g}$ in Equation (5), such that $kr'^2 \to kr'^2 + \int_{r'}^\infty 2GM(r)/(c^2r^2)dr$ with $t \approx t_0$. In other words, GR is only (locally) valid with respect to the background metric (R. Monjo 2024), and thus gravity dynamics is due to the perturbation term $\hat{h} \coloneqq \hat{g} - g$,

$$g_{\rm Sch} :\approx \eta + (\hat{g} - g) \approx \left(1 - \int_{r'}^\infty \frac{2GM(r)}{c^2r^2}dr\right)c^2dt^2 - \left[\left(1 + \int_{r'}^\infty \frac{2GM(r)}{c^2r^2}dr\right)dr'^2 + r'^2 d\Sigma^2\right]. \quad (6)$$

2. The coordinates that parameterize the metric are finally projected as follows:

$$r' \to \hat{r}' = \lambda^{1/2} r'$$
$$t \to \hat{t} = \lambda t,$$

where $\lambda \coloneqq 1/(1-\gamma/\gamma_0)$ is the stereographic scaling, which is a function of the angular position $\gamma = \sin^{-1}(r'/t_0)$ and a projection factor $\gamma_0^{-1} = \gamma_{\rm sys}^{-1}\cos\gamma_{\rm sys}$, where $\gamma_{\rm sys}$ is the characteristic angle of the gravitational system. In an empty Universe, $\gamma_0 = \gamma_U/\cos\gamma_U$. We expect $\gamma_U = \frac{1}{3}\pi$ and therefore that $\gamma_0 = \frac{2}{3}\pi \approx 2$ (R. Monjo & R. Campoamor-Stursberg 2023).

With these ingredients, the minimally perturbed metric derived by HMG outside a distribution mass is (Appendix A)

$$\hat{g} \approx \left(1 - \frac{2GM}{c^2 r} + \frac{2r}{\gamma_0(r)ct}\right)c^2dt^2 - \left[\left(1 + \frac{2GM}{c^2 r} + \frac{2r}{\gamma_0(r)ct}\right) \times dr^2 + r^2\left(1 + \frac{r}{\gamma_0(r)ct}\right)d\Sigma^2\right], \tag{7}$$

where $r/\gamma_0(r)$ approaches 0 for both $r \to 0$ and $r \to \infty$. Alternatively, comoving radial coordinate $r' \equiv (t_0/t)\, r$ can be used instead of r, but it is assumed to be approximately equivalent for gravitational systems close to the observers.

The spacetime derived from local GR (that is, resulting in Equation (6)) and the one represented by the perturbed metric (Equation (7)) satisfy the requirement to be asymptotically flat and coincide with the diagonal Schwarzschild solution at large distances. Therefore, the effective "enclosed mass" can be estimated as usual in weak lensing (M. Bartelmann & P. Schneider 2001; C. M. Will 2014; K. Umetsu 2020). To illustrate the behavior of Equation (7) for weak gravitational fields, an example of deflection angles is derived in Appendix B.

2.3. Orbital Speed and Hubble Flux Relation

The orbital speed v_C is modeled by HMG according to the geodesic equations obtained for the projected time component of the perturbation $\hat{h}_{tt}$. As a result, a fictitious cosmic acceleration of $a_{\gamma 0}(r) \coloneqq \gamma_0(r)^{-1} 2\, c/t = \gamma_{\rm sys}^{-1}(r)\cos\gamma_{\rm sys}(r)\, 2\, c/t$ emerges with a nonnegligible time-like component, which contributes to a more effective gravity with a total centrifugal acceleration $a_C(r) = v_C^2/r$ such that (Appendix A)

$$a_C(r)^2 \approx a_{\rm N}(r)^2 + |a_{\rm N}(r)|\frac{2c}{\gamma_0(r)t} \Rightarrow \left(\frac{v_C}{v_{\rm N}}\right)^2 \approx \sqrt{1 + \frac{1}{|a_{\rm N}|}\frac{2c}{\gamma_0(r)t}}, \tag{8}$$

where $a_{\rm N}(r) \coloneqq GM_{\rm sys}/r^2$ is the Newtonian acceleration and $v_{\rm N} = \sqrt{a_{\rm N}(r)r}$ is the circular orbital speed, while the last term (which depends on γ_0) represents an additional contribution to the gravitational acceleration. Notice that Equation (8) leads to $v_{\rm flat} = \lim_{r\to\infty} v_C = [2GM_{\rm sys}c/(\gamma_0 t)]^{1/4}$ as in Equation (1). However, assuming that gravitationally bounded space does not expand (i.e., $r'(t_0) \mapsto r(t) = r'(t_0)$ does not increase) as a function of time $t_0 \mapsto t > t_0$, one could require using the redshift z for estimating the observed time $t \mapsto t_0 \approx t/(1 + z/2)$ in the gravitational system (R. Monjo 2024).

For modeling observations of circular orbital velocities, the characteristic angle $\gamma_{\rm sys}$ of the considered system can be estimated from a general approach by considering the relative geometry (angle) between the Hubble speed $v_{\rm H}(r) \coloneqq r/t$ and the Newtonian circular speed $v_{\rm N}(r) \coloneqq \sqrt{GM_{\rm sys}/r}$, as follows (R. Monjo & I. Banik 2024):

$$\sin^2\gamma_{\rm sys}(r) \approx \sin^2\gamma_U + (\sin^2\gamma_{\rm center} - \sin^2\gamma_U) \times \left|\frac{2v_{\rm N}^2(r) - \epsilon_{\rm H}^2 v_{\rm H}^2(r)}{2v_{\rm N}^2(r) + \epsilon_{\rm H}^2 v_{\rm H}^2(r)}\right|, \tag{9}$$

where the parameter $\epsilon_{\rm H}^2$ is the so-called relative density of the neighborhood, while $\gamma_{\rm center} \approx \pi/2$ and $\gamma_U = \pi/3$ can be fixed here to set a one-parameter ($\epsilon_{\rm H}$) general model from Equation (9) instead of fitting an average value γ_0 in the simple γ-HMG version (Equation (8)).

The interpretation of Equation (9) is the following: The additional contribution to the gravity in galaxy rotation curves is minimal when the projective angle is maximal (i.e., $\gamma_{\rm sys} = \gamma_{\rm center}$), reached for the highest velocities $v_{\rm N} \gg \epsilon_{\rm H} v_{\rm H}$ at small radial distances (i.e., recovering the classical Newtonian regimen). In contrast, the additional contribution is maximum with minimum angle, $\gamma_{\rm sys} = \gamma_U$, when the Newtonian speed is reduced down to the Hubble flux $v_{\rm N} = \epsilon_{\rm H} v_{\rm H}$ at larger distances (bordering with neighbor systems). Therefore, the model described by Equation (9) consists of a key parameter $\epsilon_{\rm H}$ that refers to the dynamical equilibrium of the neighborhood (that is, $v_{\rm N} = \epsilon_{\rm H} v_{\rm H}$) and modulates the more effective gravity.

In other words, the parameter ϵ_H is not totally free, since it is theoretically and statistically strongly linked to the observed density $\rho(r)$ of the system at $r = r_{\rm nei} \sim 50$–200 kpc, which are neighborhood distances $r_{\rm nei}$ with dynamical equilibrium (R. Monjo & I. Banik 2024). In particular, for a typical distance $r_{\rm sys} < r_{\rm nei}$, we found that $\frac{1}{6} \leqslant \epsilon_H^2(r_{\rm sys}) \leqslant \frac{1}{6} + \rho(r_{\rm nei})/\rho_{\rm vac}$, where $\rho_{\rm vac} \coloneqq 3/(8\pi G t^2)$ is the vacuum density. To test its impact on the model, we considered two approaches in this work. On the one hand, we set $\gamma_0(r) = \gamma_0$ as a characteristic constant (at least for each type of system) to simply fit a one-parameter γ-HMG model (Equation (8)) in a similar way to that in the MOND paradigm. On the other hand, we assume an ϵ-HMG version in which $\gamma_0(r) = \gamma_{\rm sys}(r)/\cos\gamma_{\rm sys}(r)$ depends on the velocities modulated by $\epsilon_{\rm H}^2$ as shown in Equation (9). In turn, $\epsilon_{\rm H}$ is presumed to vary as a function of the system density $\rho(r_{\rm sys})$ at a given distance $r_{\rm sys}$, as follows:

$$\epsilon_{\rm H}^2(r_{\rm sys}) - \frac{1}{6} \approx \left(\frac{\rho(r_{\rm nei})}{\rho_{\rm vac}}\right)^{\zeta} = \left(\frac{\rho(r_{\rm sys})}{\rho_{\rm vac}}\right)^{\zeta}\left(\frac{r_{\rm sys}}{r_{\rm nei}}\right)^{3\zeta}, \tag{10}$$

where $\zeta = 1$ is theoretically derived but a range is empirically found about $0.8 < \zeta \leqslant 1$ (R. Monjo & I. Banik 2024). Therefore, the semiempirical ϵ-HMG has two parameters, ζ and $r_{\rm nei}/r_{\rm sys} \geqslant 1$, which modulate the equilibrium of the gravitational system (Figure 1).

Notice that when $\zeta = 1$ and $r = r_{\rm sys}$ with $\epsilon_{\rm H} \gg \frac{1}{6}$, the ϵ-HMG model is equivalent to the simplest γ-HMG version, for which the Hubble–Newton dynamical equilibrium ($\gamma_{\rm sys} = \gamma_U$) is reached at $r = r_{\rm sys} = r_{\rm nei}$ in Equation (9), as was found for some galaxies in the same study. In contrast, if $\zeta < 1$, the system is not in equilibrium for $r = r_{\rm sys}$ under the ϵ-HMG approach (Equations (9) and (10)). Thus, we set $\zeta \approx 0.8$ to estimate $r_{\rm nei}/r_{\rm sys}$ for galaxies whose circular orbital speed is clearly higher than the Hubble flux. Finally, flat velocities were modeled by fitting a_0 in MOND and $\gamma_{\rm sys}$ in γ-HMG, since these constant speeds are independent of radial distances owing to

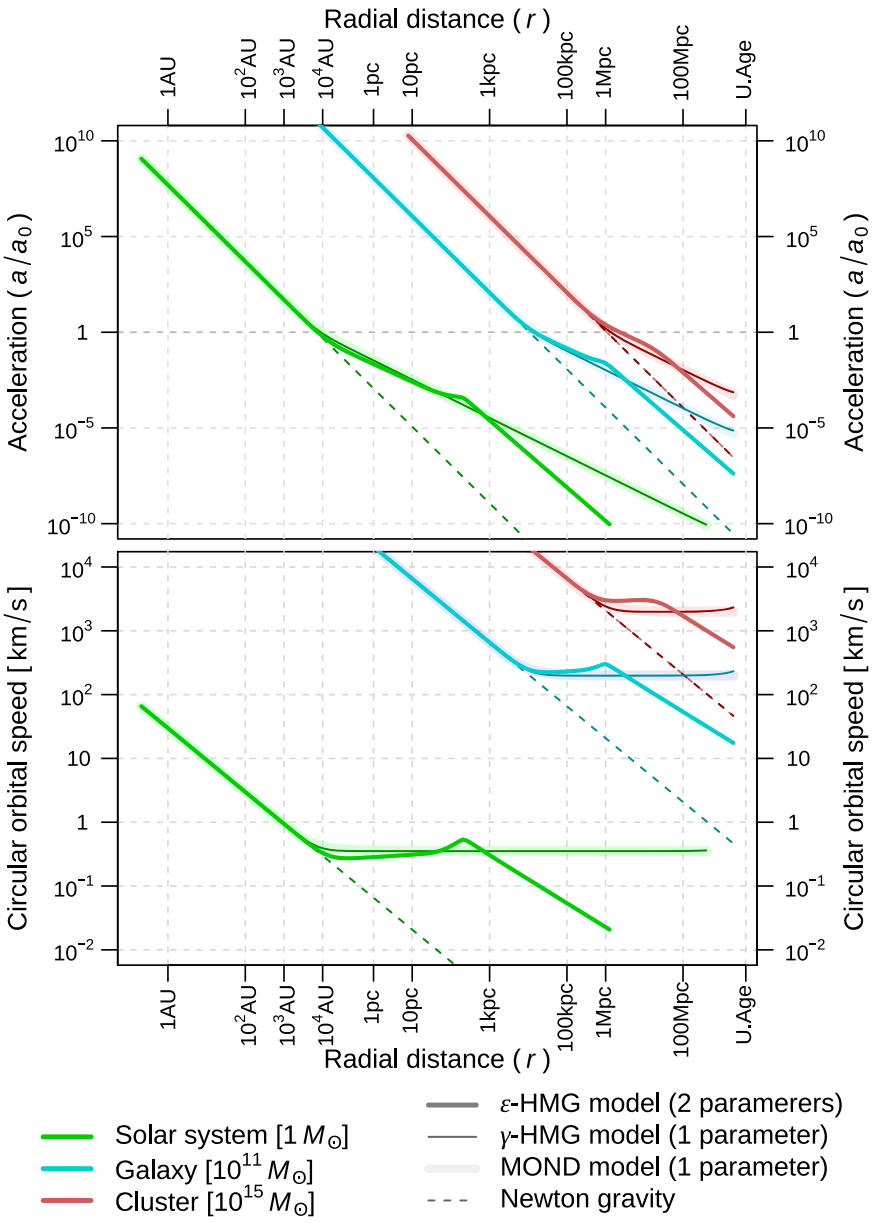

Figure 1. Example of acceleration (top panel) and circular orbital speed (bottom panel) curves, as a function of the radial distance (r), for three gravitational systems centered, respectively, by three characteristic baryonic masses enclosed in r: Sun (1 $M_\odot$; green), galaxy (10^{11} $M_\odot$; blue), and galaxy cluster (10^{15} $M_\odot$; red). The models used are the classical Newtonian gravity (dashed lines), an empirical MOND function (Equation (4) with standard $a_0 = 1.2 \times 10^{-10}$ m s^{-2}; lightly colored wide lines), γ-HMG (Equation (8) with $\gamma_0 = 12$; darkly colored thin lines), and ϵ-HMG (Equations (9) and (10) with $r_{sys} \equiv r$ and different values of r_{nei}/r_{sys} and ζ; darkly colored wide lines). The represented ϵ-HMG configurations (r_{nei}/r_{sys}, ζ) are (4, 0.9) for the solar system, (3, 0.9) for the galaxy, and (2, 0.9) for the cluster. The value of $\zeta \equiv 1$ implies that a gravitational system is close to equilibrium with respect to the Hubble flux. The radial distances (r) range between 1 au and the maximum light-travel distance ($t_0 c$) given by the age t of the Universe (noted as "U. Age," which is $t_0 c \approx 13.7$ Gly with $c \equiv 1$).

their own asymptotic definition (i.e., ϵ-HMG cannot be adequately fitted).

3. Results and Discussion

3.1. General Findings

The γ-HMG and ϵ-HMG versions of the model and their derived dynamics illustrate the motion of circular orbits in a modified spacetime, reflecting both classical Newtonian and nonclassical gravitational effects due to a distorting acceleration of about $c/(\gamma_0 t) \lesssim 10^{-10}$ m s^{-2}. The resulting new terms represent cosmic influences on gravitational phenomena that should be observable in large-scale astrophysical contexts, as our results suggest.

Without considering redshift effects, the best γ-HMG model fitted to *flat* velocities is found for $\gamma_0 = 8.2^{+1.1}_{-0.9}$, which is compatible with the lowest value of $\gamma_0 = 9.8^{+1.6}_{-1.3}$ fitted to circular velocities (Table 1, Figures 2 and 3). This fact is not coincidental because γ_0 is not a constant in the HMG paradigm since it decreases for galaxies (Equation (9)), as the radius increases with an almost flat velocity. Similar results are found when the redshift effect is considered: the lowest value of the projection factor for circular velocities ($\gamma_0 = 11.9^{+1.9}_{-1.6}$) is very close to the one obtained for *flat* velocities ($\gamma_0 = 9.8^{+1.2}_{-1.1}$).

On the other hand, the MOND parameter $a_0 = 1.21^{+0.14}_{-0.13} \times 10^{-10}$ m s^{-2} fitted to circular velocities is incompatible with the *flat* velocities analyzed in this work (Figure 3)

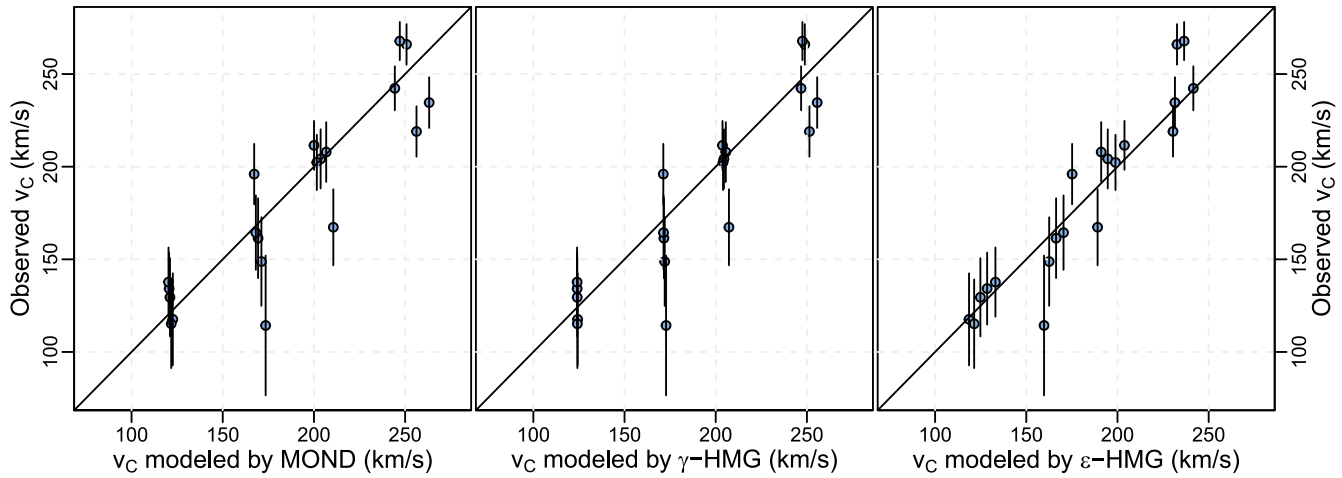

Figure 2. Modeling of circular speed assuming the current time $t \approx t_0$ (i.e., no redshift effects) according to an empirical MOND function (Equation (4) with $a_0 = 1.21 \times 10^{-10}$ m s^{-2}; left panel), γ-HMG (Equation (8) with $\gamma_0 = 9.8$; middle panel), and ϵ-HMG (Equations (9) and (10) with $\zeta = 0.8$ and $r_{\rm nei}/r_{\rm sys} = 2.5$; right panel). These models are fitted to the observed circular velocity inferred from weak lensing (Table 1 of T. Mistele et al. 2024). Data are gathered in four sets according to four baryonic mass bins (1.29, 4.57, 9.13, and 19.5 in units of 10^{10} $M_\odot$).

Table 1
Fitting Parameters of Empirical MOND Interpolation (Equation (4)), γ-HMG (Equation (8) with $\gamma_0 =$ Constant), and ϵ-HMG (Equations (9) and (10) with $\zeta = 0.8$) Models to Observed Circular and Flat Velocities Inferred from Weak Lensing (T. Mistele et al. 2024)

Method	Velocity Data	Parameter	χ^2 (p-value)	Best One (*)
MOND	circular	$a_0 = 1.21^{+0.14}_{-0.13} \times 10^{-10}$ m s^{-2}	31.3 (0.96)	⋯
γ-HMG	circular	$\gamma_0 = 9.8^{+1.6}_{-1.3}$	25.7 (0.86)	⋯
γ-HMG + z	circular	$\gamma_0 = 11.9^{+1.9}_{-1.6}$	25.9 (0.87)	⋯
ϵ-HMG	circular	$r_{\rm nei}/r_{\rm sys} = 2.5^{+0.5}_{-0.4}$	18.0 (0.48)	⋯
ϵ-HMG + z	circular	$r_{\rm nei}/r_{\rm sys} = 2.9^{+0.7}_{-0.5}$	17.5 (0.44)	*
MOND	flat	$a_0 = 1.63^{+0.23}_{-0.20} \times 10^{-10}$ m s^{-2}	26.1 (0.38)	⋯
γ-HMG	flat	$\gamma_0 = 8.2^{+1.1}_{-0.9}$	24.5 (0.30)	*
γ-HMG + z	flat	$\gamma_0 = 9.8^{+1.2}_{-1.1}$	25.0 (0.32)	⋯

Note. The symbol z is added when redshift is considered via $t_0 \approx t/(1 + z/2)$ in the fitting of γ-HMG and ϵ-HMG.

and is 3σ separated with respect to the best fit ($a_0 = 1.63^{+0.23}_{-0.20} \times 10^{-10}$ m s^{-2}). This MOND-based best fit presents a poor result (χ^2 p-value > 0.95) in 2σ tension with respect to the standard value of $a_0 = 1.2 \times 10^{-10}$ m s^{-2}, which is assumed to be a universal constant. Moreover, the fitting of the ϵ-HMG model showed qualitatively better results in explaining the circular velocities self-consistently compared to the MOND and γ-HMG models (Figure 2).

The impact of the redshift on the above findings is not statistically significant for modeling observations of circular orbital velocities (Table 1 and Figure 2). The explanation is that gravity strongly binds its spatial coordinates, mostly removing the effect of expansion, so $r = r'$. In contrast, the flat velocity $v_{\rm flat}$ approaches the external limit of the gravitational force, and therefore the Hubble law $r'/t_0 \approx r/t$ is approximately satisfied. From this effect, the observed cosmic acceleration is practically invariant under the observable time periods (i.e., the dependence on redshift is weak). This finding is consistent with emergent data on the rotation curves of disk galaxies at significant redshifts (J. D. Bekenstein & E. Sagi 2008; S. S. McGaugh et al. 2016).

3.2. Limitations of the Current HMG Model

The standard ΛCDM model has achieved numerous successes such as the ability for reproducing the perturbation spectrum in the cosmic microwave background (CMB), the observed large-scale structure of the Universe, and the formation of galactic structures among other astrophysical observations (S. Dodelson 2003; P. Li et al. 2020). It is well established that purely baryonic disk galaxies, in the absence of DM halos, are highly susceptible to bar instabilities and excessive spiral structure growth. Numerical simulations and theoretical studies have consistently shown that disk galaxies without a stabilizing mass component tend to develop bars and rapidly evolve away from their observed morphologies (J. P. Ostriker & P. J. E. Peebles 1973; G. Efstathiou et al. 1982; M. D. Weinberg & N. Katz 2002).

Any modified gravity should count whether it can stabilize the disks against bar formation. O. Tiret & F. Combes (2007) explored the performance of MOND in structure formation and found that galactic disks experience bar instability earlier than the DM model. Additionally, the evolution of bar pattern speed differs significantly because MOND systems experience significantly weaker dynamical friction compared to equivalent

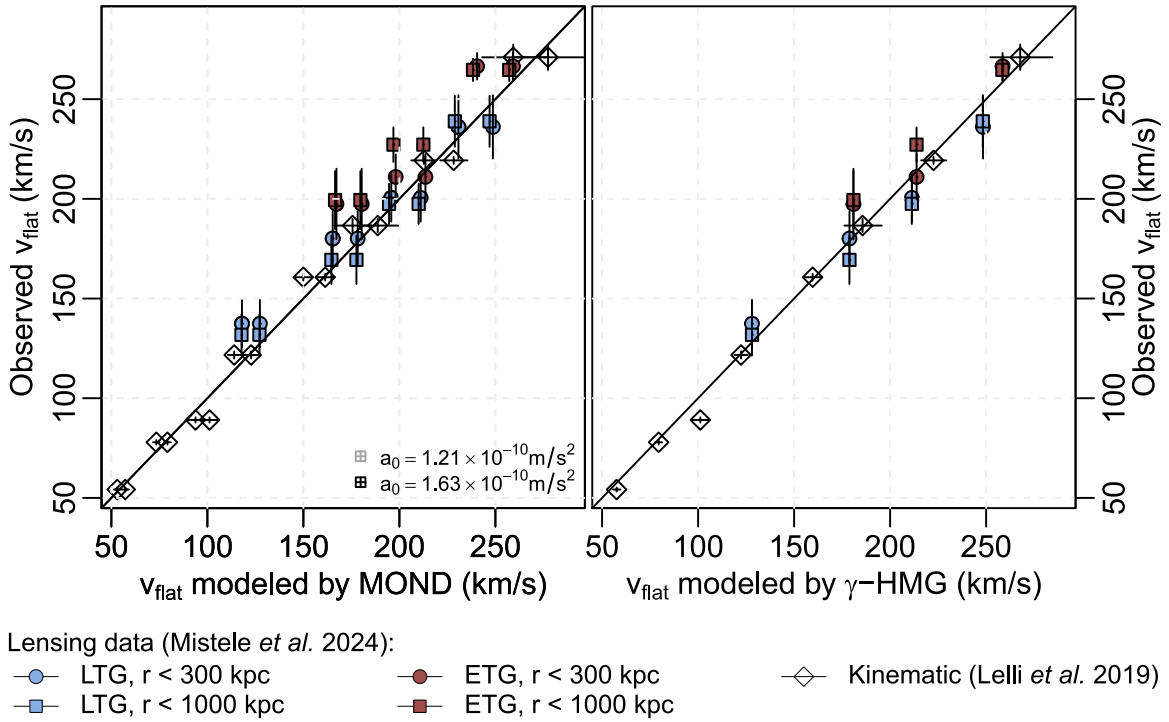

Figure 3. Flat velocity (asymptotic speed of the rotation curve) according to weak-lensing observations for ETGs and LTGs separately (red and blue symbols; T. Mistele et al. 2024) and kinetic data (white diamonds; F. Lelli et al. 2019). The left panel shows values from the empirical MOND function with $a_0 = 1.21 \times 10^{-10}$ m s^{-2} (light colors) fitted with circular speeds (Table 1) and with $a_0 = 1.65 \times 10^{-10}$ m s^{-2} (dark colors) fitted to flat velocities. The right panel shows the γ-HMG model fit to flat velocities with $\gamma_0 = 8.2$.

Newtonian systems (i.e., with the same phase-space distribution of baryons and DM; C. Nipoti et al. 2008).

Since HMG recovers the MOND regimen for most of the observed galaxy dynamics, it is probably challenged to stabilize the formation of galactic systems. Therefore, it is necessary to analyze how HMG may (or may not) offer a natural stabilization mechanism without the need for DM halos. The mechanism of fictitious acceleration (which emerges from the cosmic background metric) could be a key to stabilization.

Another critical point is that systems of comparable mass exhibit distinct dynamical properties, which result in different needs (or no need) for DM components. For example, ultrafaint galaxies, within the framework of Newtonian gravity, are among the most DM-dominated systems, exhibiting exceptionally high inferred DM-to-baryon ratios, often exceeding those estimated for galaxy clusters (J. D. Simon 2019). In contrast, some globular clusters with a mass range similar to that of many ultrafaint galaxies do not appear to require a significant DM component (B. Moore 1996; D. A. Forbes et al. 2018). One notable example is the galaxy NGC 1052-DF2, which has been observed to have an unusually low DM content (H. Baumgardt & M. Hilker 2018; D. A. Forbes et al. 2018). This striking diversity raises a fundamental question that HMG should address in future work. A possible way to solve this issue could be the proposal of R. Monjo & I. Banik (2024), who explored the ability of HMG for reproducing a multiscale range of distances, accelerations, and orbital velocities.

However, the standard DM-based model also presents difficulties in explaining some open issues. For example, numerical simulations predict that DM halos should have central cusps, while those inferred from observed galaxies do not have cusps (M. D. Weinberg & N. Katz 2002). Moreover, the observed number of small galaxies and dwarf satellite systems in the Local Group is significantly lower than the predicted abundance of low-mass DM halos and subhalos within comparable volumes. These discrepancies contribute to some of the most well-known challenges faced by the ΛCDM paradigm, including the cusp/core problem, the missing satellites problem, and the too-big-to-fail issue (J. S. Bullock & M. Boylan-Kolchin 2017). The lack of direct detection of DM and the problems in modeling structures such as the impossible early galaxies (M. K. Yennapureddy & F. Melia 2018), the Giant Arc and Big Ring (A. M. Lopez et al. 2024), or the El Gordo collision (E. Asencio et al. 2023) could promote the development of alternatives such as the HMG model or other MOND-like theories (P. Kroupa 2015; E. Asencio et al. 2022; P. Kroupa et al. 2023). For example, the Hubble tension on the different acceleration rates of the Universe could be addressed by the fictitious acceleration that emerges from the hyperconical model, which is used as a basis for the HMG (R. Monjo 2018, 2024).

Hence, it is essential to investigate whether the HMG model naturally leads to solving some of the above problems, including a wide range of multiscale structure formation, with adequate stability.

4. Concluding Remarks

According to the HMG model, the Newtonian gravitational acceleration is modified by a distorting term $c/(\gamma_0 t)$ that represents a fictitious acceleration inherited from the large-scale effects of comoving reference frames. The modified gravity results in an additional multiscale cosmic acceleration offset but with a special print on galactic dynamics. It is worth recalling that gravitational lensing is derived from deviations in the metric geodesics, with a deeper curvature that would be

caused by DM or by a more efficient gravity from baryonic matter.

The analysis of circular velocities inferred from weak-lensing observations suggests the viability of HMG as an alternative to the DM paradigm, providing a relativistic cosmic approach to the MOND regime. By fitting the observed data to the model, we demonstrate that HMG can reproduce the flat velocity curves even for the 1 Mpc scale, without requiring unobservable particles. Our findings showed that the circular and flat rotation curves are statistically independent of the redshift, which suggests that the coupling of the cosmic acceleration to the perturbed metric in the local GR is very weak. However, the wide-scale flexibility of fitting and the cosmological basis of HMG provide a consistent and potentially more fundamental explanation for the observed gravitational phenomena in galaxies. Although our preliminary findings reinforce the viability of the theory, future studies with larger data sets and more refined versions are needed to validate these results and explore the full implications of HMG for our understanding of cosmology and gravity. Complementary work is now being carried out aligned with reproducing the CMB spectrum and the big bang nucleosynthesis using the timeline simulated by R. Monjo & R. Campoamor-Stursberg (2023). In future works, we will explore whether effective modifications of the gravitational potential induced by the fictitious acceleration of HMG could contribute to disk stability. Moreover, we will examine the ability of HMG to predict the correct behavior of merging clusters and to reproduce observations such as the Bullet Cluster or El Gordo collisions, among other large-scale structures.

Acknowledgments

The authors thank T. Mistele for providing all the necessary data for this study, as well as for all comments and suggestions. We also acknowledge our colleague I. Banik for the valuable feedback and discussions, especially on the interpretation of multiscale behavior of the HMG model. Finally, we greatly appreciate the very constructive comments of the reviewers, which have helped to improve this article.

Data Availability

In this study, no new data were created or measured.

Appendix A
Minimally Perturbed Metric and Circular Orbital Velocity

This appendix derives the low acceleration limit from the weak-perturbed field given by the hyperconical model and examines the geodesic equations. Let g be a first-order metric obtained from local GR assuming an approximately unitary scale factor ($t/t_0 \approx 1$) for gravitational systems with mass $M(r')$ enclosed in the radial coordinate r' (R. Monjo 2024):

$$g \approx \left(1 - \int_{r\prime}^{\infty} \frac{2GM(r)}{c^2 r^2} dr\right) dt^2 - \left(1 + \int_{r\prime}^{\infty} \frac{2GM(r)}{c^2 r^2} dr\right) dr'^2 - r'^2 d\Sigma^2, \quad \text{(A1)}$$

where Σ represents the angular coordinates with $d\Sigma = \sin\theta\, d\theta\, d\phi$. For instance, consider the simplest case with perturbation compatible with the $1/2$-distorting stereographic projection of R. Monjo & R. Campoamor-Stursberg (2023), which is obtained from the following differential transformations assuming an almost constant $\gamma_0 = \gamma_0(r') \geqslant 2$:

$$r' \to \hat{r}' \approx \left(1 + \frac{r'}{2\gamma_0(r')ct_0}\right) r'$$
$$\Rightarrow \quad dr' \to d\hat{r}' \approx \left(1 + \frac{r'}{\gamma_0(r')ct_0}\right) dr' \quad \text{(A2)}$$

$$t \to \hat{t} \approx \left(1 + \frac{r'}{\gamma_0(r')ct_0}\right) t$$
$$\Rightarrow \quad dt \to d\hat{t} \approx \left(1 + \frac{r'}{\gamma_0(r')ct_0}\right) dt + \text{ neglected terms}. \quad \text{(A3)}$$

Substituting these transformations into the metric $g = g_{ij} dx^i dx^j$, the resulting minimally perturbed metric $\hat{g}$ is

$$\hat{g} \approx \left(1 - \int_{r'}^{\infty} \frac{2GM(r)}{c^2 r^2} dr + \frac{2r'}{\gamma_0 ct_0}\right) c^2 dt^2 - \left[\left(1 + \int_{r\prime}^{\infty} \frac{2GM(r)}{c^2 r^2} dr + \frac{2r'}{\gamma_0 ct_0}\right) dr'^2 + r'^2 \left(1 + \frac{r'}{\gamma_0 ct_0}\right) d\Sigma^2\right]. \quad \text{(A4)}$$

To analyze cosmic effects, we define an expanding coordinate $r \equiv (t/t_0) r'$, which is practically indistinguishable from the comoving coordinate r' for gravitational systems, but it is a key for large scales. Therefore, the approaches $\frac{2GM}{c^2 r'} \approx \frac{2GM}{c^2 r} \ll 1$ and $\frac{2r'}{\gamma_0 ct_0} \approx \frac{2r}{\gamma_0 ct} \ll 1$ are assumed for the weak-field limit.

According to GR, the geodesic equations are expressed as $\ddot{x}^\mu + \Gamma^\mu_{\nu\sigma} \dot{x}^\nu \dot{x}^\sigma = 0$, where $\Gamma^\mu_{\nu\sigma} \equiv \frac{1}{2} g^{\mu\lambda} (\partial_\sigma g_{\lambda\nu} + \partial_\nu g_{\lambda\sigma} - \partial_\lambda g_{\nu\sigma})$ are the Christoffel symbols and $\dot{x}^\mu \equiv dx^\mu/d\tau$ is the derivative by the proper time τ. The geodesic equations can also be derived from the Lagrangian $\mathcal{L} = (g_{\mu\nu} \dot{x}^\mu \dot{x}^\nu)^{1/2}$ that provides the Euler–Lagrange equations $\frac{d}{d\tau}(\partial\mathcal{L}/\partial\dot{x}^\mu) - \partial\mathcal{L}/\partial x^\mu = 0$. From this approach, a classical-like conservation of the energy E is easily found as follows:

$$E \approx \left(1 - \int_r^{\infty} \frac{GM(r')}{c^2 r'^2} dr' + \frac{r}{\gamma_0 ct} - \frac{1}{2}\frac{\nu^2}{c^2}\right) m_0 c^2, \quad \text{(A5)}$$

where m_0 is the mass of a test particle and ν is its speed. Since secondary terms of $cdt/d\tau \approx 1 + GM/(c^2 r) - r/(\gamma_0 ct) \approx 1$ only contribute to negligible terms in the geodesic equations, total acceleration of a test particle placed at the position $s = te_t + re_r$ with respect to a mostly central mass M is

$$a_s \equiv \frac{d^2 s}{c^2 dt^2} \approx \frac{d^2 s}{d\tau^2} \approx -\frac{r}{\gamma_0 ct^2} e_t - \left(\frac{GM}{c^2 r} + \frac{1}{\gamma_0 ct}\right) e_r. \quad \text{(A6)}$$

The interpretation of Equation (A6) is that centrifugal acceleration should also have both time-like and space-like components. Specifically, the time-like component of the acceleration measured by an observer living in the hyperconical Universe is expected to be proportional to $1/(ct)$, as the spatial contribution is proportional to $1/r$. Therefore, total centrifugal

acceleration should be

$$a_s = \frac{d^2s}{c^2dt^2} = -\frac{\omega_t^2}{c^2}ct\ e_t - \frac{\omega_r^2}{c^2}r\ e_{\vec{r}} = -\frac{1}{ct}\frac{v_t^2}{c^2}\ e_t - \frac{1}{r}\frac{v_r^2}{c^2}\ e_{\vec{r}}, \tag{A7}$$

where $\omega_t^2 \equiv v_t^2/(ct)^2$ and $\omega_r^2 \equiv v_r^2/r^2$ are the squared angular speeds in the time- and space-like directions, respectively, while v_t^2 and v_r^2 are tangential squared speeds. Finally, we hypothesize that observers measure an effective centrifugal acceleration given by an apparent circular orbital speed v around a radial distance r, as

$$||a_s|| = \frac{1}{r}\frac{v^2}{c^2} = -\frac{1}{r}\left|\left|\frac{v_t^2}{c^2}\ e_t + \frac{v_r^2}{c^2}\ e_{\vec{r}}\right|\right|. \tag{A8}$$

Thus, taking into account Equations (A6) and (A7), the absolute value of the speed v is given by

$$\frac{v^4}{c^4} = -\left|\left|\frac{v_t^2}{c^2}\ e_t + \frac{v_r^2}{c^2}\ e_{\vec{r}}\right|\right|^2 \approx -\left[\left(\frac{r}{\gamma_0 ct}\right)^2 - \left(\frac{GM}{c^2r} + \frac{r}{\gamma_0 ct}\right)^2\right] \approx \left(\frac{GM}{rc^2}\right)^2 + \frac{2GM}{\gamma_0 tc^3},$$

which satisfies two well-known limits of Newton's dynamics and the Milgrom's MOND:

$$v \approx \sqrt{\frac{GM}{r}} \qquad \text{if } a_N(r) \gg \frac{2c}{\gamma_0 t} \simeq a_0 \tag{A9}$$

$$v \approx \sqrt[4]{\frac{2GMc}{\gamma_0 t}} \qquad \text{if } a_N(r) \ll \frac{2c}{\gamma_0 t} \simeq a_0, \tag{A10}$$

where $a_N(r) \equiv GM/r^2$ is the classical Newtonian acceleration, a_0 is Milgrom's constant acceleration, and $M = M(r)$ is the total mass within the central sphere of radius r. Notice that the velocity curve $v = v(r)$ can be reworded in terms of the Kepler–Newton speed $v_N(r) \coloneqq \sqrt{GM(r)/r}$, leading to an MDAR:

$$v^4 = v_N^4 + v_N^2\, r\frac{2c}{\gamma_0 t} \quad \Rightarrow \quad \frac{M_{\rm eff}(r)}{M(r)} = \frac{v^2(r)}{v_N^2(r)} = \sqrt{1 + \frac{1}{|a_N(r)|}\frac{2c}{\gamma_0 t}}, \tag{A11}$$

where $M = r\ v_N^2/G$ is the baryonic mass and $M_{\rm eff} = r\,v^2/G$ is the apparent total or effective mass.

Appendix B
Deflection Angle in HMG

This appendix summarizes the method of G. W. Gibbons & M. C. Werner (2008) based on the Gauss–Bonnet theorem to derive the deflection angle ($\hat{\varphi}$) by integrating the Gaussian curvature (K) over a domain exterior to the lens, thus providing a geometrically insightful perspective on gravitational lensing by using its related optical metric. The Gauss–Bonnet theorem describes the geometry of a surface D in relation to its topology, which is given by

$$\iint_D K\ dA + \oint_{\partial D} \kappa_g\ ds + \sum_i \theta_i = 2\pi\chi(D) \quad \Rightarrow \quad \text{Weak lensing: } \hat{\varphi} \equiv \sum_i \theta_i = -\iint_{D_2} K\ dA, \tag{B1}$$

where k_g is the geodesic curvature, α_i are the exterior angles, and $\chi(D)$ is the Euler characteristic for a domain D. For weak gravitational lensing, the Gaussian curvature K is related to the gravitational potential around the lensing mass. The geodesic curvature k_g is typically zero along the asymptotically flat boundary at infinity, contributing negligibly to the theorem. The exterior angles α_i account for the deficit angles due to spacetime curvature, directly relating to the light deflection angle $\hat{\varphi}$, where $\sum_i \alpha_i = -\varphi$. The Euler characteristic $\chi(D)$ of the exterior domain is zero because the domain is noncompact and asymptotically resembles a flat plane with holes. By integrating the Gaussian curvature and accounting for the exterior angles, Gibbons and Werner's method effectively captures how light bends around a gravitational lens, providing a straightforward and intuitive framework for calculating lensing effects in weak gravitational fields (Z. Li & T. Zhou 2020).

In our case, let $g = g_{tt}dt^2 + g_{rr}dr^2$ be the metric defined by Equation (A4). Both the g_{tt} and g_{rr} components contribute to the deflection angle of light. However, the time dilation represented by g_{tt} plays a dominant role in determining the amount of bending that occurs, particularly because it directly represents the gravitational influence on the energy of photons. Finally, the interaction between the time dilation and spatial curvature effects (via the optical metric σ) leads to the observable phenomenon of gravitational lensing. Therefore, in weak-field approximations, where $2GM/c^2 \ll 1$, the Newtonian-like potential (from g_{tt}) gives the leading contribution to light bending, consistent with the classical expectation that gravity acts as a potential well that bends paths in its vicinity. Specifically, the optical metric σ related to g is defined by the null geodesics ($ds^2 = g'_{ij}dx^i dx^j = 0$), and simplifying for the equatorial plane ($\theta = \pi/2$) outside the mass distribution, it is given by:

$$\sigma = \frac{g_{rr}}{g_{tt}}\,dr^2 + \frac{g_{\phi\phi}}{g_{tt}}\,d\phi^2 \approx \left(1 + \frac{4GM}{c^2r}\right)dr^2 + r^2\left(1 + \frac{2GM}{c^2r} - \frac{r}{\gamma_0(r)\ c\ t(r)}\right)d\phi^2, \tag{B2}$$

where Maclaurin expansion was used for the smallest terms and $t(r) = t_0 - r/c$ is considered to model effects from the early epochs of the Universe. Assuming that $\partial_r \gamma_0(r) \ll \gamma_0(r)/r$, the Gaussian curvature K is dominated by the crossing derivatives of (r, ϕ) over the components $\sigma_{\phi\phi} = g_{\phi\phi}/g_{tt}$ that are given by the Riemann tensor $R_{r'\theta r'\theta}$ of the optical metric σ, that is,

$$K = -\frac{R_{r\theta r\theta}}{\det\sigma} \approx \frac{2GM}{c^2r^3} + \frac{1}{\gamma_0(r)\ r\ c\ t(r)}, \tag{B3}$$

where $\gamma_0(r) = \gamma_{\rm sys}(r)/\cos\gamma_{\rm sys}(r)$ and $\det\sigma = \sigma_{rr}\sigma_{\phi\phi} \approx 1$ is the determinant of the optical metric. The vacuum value of the projective factor is approximately $\gamma_0(r) \approx 2$ (R. Monjo & R. Campoamor-Stursberg 2023).

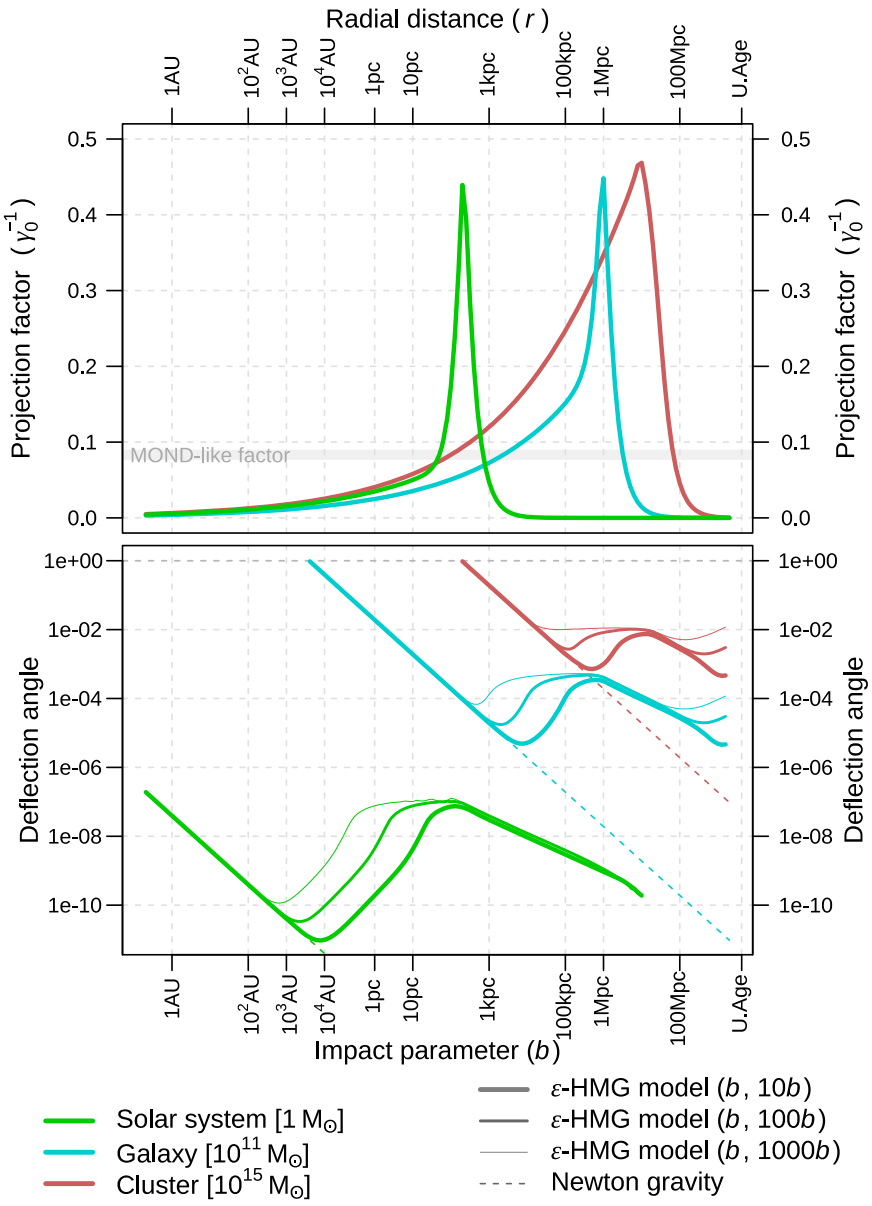

Figure B1. Example of projection factor (top panel) and corresponding deflection angle in radians (bottom panel) as a function of the impact factor (b) equal to the radial distance (r), for three gravitational systems centered, respectively, by three characteristic baryonic masses enclosed in r: Sun (1 $M_\odot$; green), galaxy (10^{11} $M_\odot$; blue), and galaxy cluster (10^{15} $M_\odot$; red). The models used are the classical Newtonian gravity (dashed lines) and ϵ-HMG (Equations (9) and (10)) with $r_{\rm sys} \equiv r$ and different values of $r_{\rm nei}/r_{\rm sys}$ and ζ; colored wide lines). The represented ϵ-HMG configurations ($r_{\rm nei}/r_{\rm sys}$, ζ) are (4, 0.9) for the solar system, (3, 0.9) for the galaxy, and (2, 0.9) for the cluster. In the top panel, a MOND-like factor of $\gamma_0^{-1} \approx 1/12$ is shown in a thick gray band to represent the Milgromian constant $a_0 \approx 2\gamma_0^{-1} c/t \approx 1.2 \times 10^{-10}$ m s^{-2}. The radial distances (r) range between 1 au and the maximum light-travel distance ($t_0 c$) given by the age t estimated for the Universe (noted as "U. Age," which is $t_0 c \approx 13.7$ Gly with $c \equiv 1$). To solve the integral of Equation (B4) in the bottom panel, the age of the Universe was considered with delay (i.e., $t \equiv t_0 - r/c$) and the domain of the radial distance (r) was ranged from b to three different maximum values: $10 \times b$ (thickest colored lines), $10^2 \times b$ (intermediate colored lines), and $10^3 \times b$ (thinnest colored lines).

Since the area element is $dA = \sqrt{g_{rr} g_{\phi\phi}}\, dr\, d\phi \approx r\, dr\, d\phi$, and integrating from $b/\sin(\phi)$ to the source of light (s.l), the deflection angle outside the mass distribution is

$$\hat{\varphi} = \int_{\delta}^{\pi-\delta} \int_{b/\sin(\phi)}^{\text{s.l.}} \left(\frac{2GM}{c^2 r^3} + \frac{1}{\gamma_0(r)\, r\, c\, t(r)} \right) r\, dr\, d\phi$$
$$\approx \frac{4GM}{c^2 b} + \int_{\delta}^{\pi-\delta} \int_{b/\sin(\phi)}^{\text{s.l.}} \frac{\cos \gamma_{\rm sys}(r)}{c\, t(r) \gamma_{\rm sys}(r)} dr\, d\phi, \qquad \text{(B4)}$$

with $0 < \delta \ll 1$ and $t(r) = t_0 - r/c$. Considering Equation (9), the contribution of the second part can be integrated by using standard numerical techniques (e.g., Simpson's rule), and it is shown in Figure B1.

For instance, the deflection angle for a typical galaxy ($M = 10^{11}$ $M_\odot$ of baryonic mass) and impact parameter $b = 10$ kpc is $\hat{\varphi}_{\rm GR} \approx 10^{-5}$ rad according to GR. However, the contribution of HMG is $\hat{\varphi}_{\rm HMG} > 10^{-4}$ rad, which could be assimilated as DM phenomenology at these distances. For the Sun ($M_\odot = 1.989 \times 10^{30}$ kg) with an impact parameter of about $b = R_\odot = 6.96 \times 10^8$ m, the deflection angle is about $\hat{\varphi}_{\rm Sun} \approx 1''.75 \approx 8.5 \times 10^{-6}$ rad, and 3.9×10^{-8} rad for $b = 1$ au. The cosmic contribution to the deflection angle

predicted by the hyperconical model is about 10^{-15} rad for these short distances, and it is only significant from the radius of 10^3 au and extends effects beyond to 10^5 au ~ 0.5 pc, which corresponds approximately to the hypothetical Oort Cloud extension (J. Crovisier 2011). Nevertheless, the predicted deflection angle for the outer solar system seems to be too large since it is extrapolated from the ϵ-HMG parameters fitted with galaxies and clusters. Therefore, a specific analysis is required in future work.

ORCID iDs

Robert Monjo https://orcid.org/0000-0003-3100-2394

References

Asencio, E., Banik, I., & Kroupa, P. 2023, ApJ, 954, 162
Asencio, E., Banik, I., Mieske, S., et al. 2022, MNRAS, 515, 2981
Banik, I., Pittordis, C., Sutherland, W., et al. 2024, MNRAS, 527, 4573
Banik, I., & Zhao, H. 2015, MNRAS, 450, 3155
Banik, I., & Zhao, H. 2022, Symm, 14, 1331
Barkana, R. 2018, Natur, 555, 71
Bartelmann, M., & Schneider, P. 2001, PhR, 340, 291
Baumgardt, H., & Hilker, M. 2018, MNRAS, 478, 1520
Bekenstein, J. D., & Sagi, E. 2008, PhRvD, 77, 103512
Blanchet, L. 2007, CQGra, 24, 3529
Brouwer, M. M., Oman, K. A., Valentijn, E. A., et al. 2021, A&A, 650, A113
Bullock, J. S., & Boylan-Kolchin, M. 2017, ARA&A, 55, 343
Clowe, D., Bradač, M., Gonzalez, A. H., et al. 2006, ApJL, 648, L109
Comerón, S., Trujillo, I., Cappellari, M., et al. 2023, A&A, 675, A143
Cookson, S. A. 2024, MNRAS, 533, 110
Crovisier, J. 2011, in Oort Cloud, ed. M. Gargaud et al. (Berlin: Springer), 1175
Di Cintio, A., & Lelli, F. 2015, MNRAS, 456, L127
Dodelson, S. 2003, Modern Cosmology (Amsterdam: Academic Press)
Dolan, B. P. 2023, Einstein's General Theory of Relativity (Cambridge: Cambridge Univ. Press)
Efstathiou, G., Lake, G., & Negroponte, J. 1982, MNRAS, 199, 1069
Forbes, D. A., Bastian, N., Gieles, M., et al. 2018, RSPSA, 474, 20170616
Frenk, C., & White, S. 2012, AnP, 524, 507
Gibbons, G. W., & Werner, M. C. 2008, CQGra, 25, 235009
Goddy, J. S., Stark, D. V., Masters, K. L., et al. 2023, MNRAS, 520, 3895
Katz, A., Reece, M., & Sajjad, A. 2016, PDU, 12, 24
Kroupa, P. 2015, CaJPh, 93, 169
Kroupa, P., Gjergo, E., Asencio, E., et al. 2023, PoS, 2022, 436
Lelli, F., McGaugh, S. S., Schombert, J. M., Desmond, H., & Katz, H. 2019, MNRAS, 484, 3267
Li, P., Dodelson, S., & Croft, R. A. C. 2020, PhRvD, 101, 083510
Li, Z., & Zhou, T. 2020, PhRvD, 101, 044043
Lopez, A. M., Clowes, R. G., & Williger, G. M. 2024, JCAP, 2024, 055
McGaugh, S. S. 2004, ApJ, 609, 652
McGaugh, S. S., de Blok, W. J. G., Schombert, J. M., de Naray, R. K., & Kim, J. H. 2007, ApJ, 659, 149
McGaugh, S. S., Lelli, F., & Schombert, J. M. 2016, PhRvL, 117, 201101
Merritt, D. 2017, SHPMP, 57, 41
Milgrom, M. 1983, ApJ, 270, 365
Milgrom, M. 2020, SHPMP, 71, 170
Mistele, T., McGaugh, S., Lelli, F., Schombert, J., & Li, P. 2024, ApJL, 969, L3
Moffat, J. W., & Toth, V. T. 2009, MNRAS, 397, 1885
Monjo, R. 2017, PhRvD, 96, 103505
Monjo, R. 2018, PhRvD, 98, 043508
Monjo, R. 2023, CQGra, 40, 235002
Monjo, R. 2024, ApJ, 967, 66
Monjo, R., & Banik, I. 2024, arXiv:2405.10019
Monjo, R., & Campoamor-Stursberg, R. 2023, CQGra, 40, 195006
Moore, B. 1996, ApJL, 461, L13
Nipoti, C., Ciotti, L., Binney, J., & Londrillo, P. 2008, MNRAS, 386, 2194
Ostriker, J. P., & Peebles, P. J. E. 1973, ApJ, 186, 467
Rodríguez-Gil, P., Gänsicke, B. T., Hagen, H.-J., et al. 2005, A&A, 431, 269
Roszkowski, L., Sessolo, E. M., & Trojanowski, S. 2018, RPPh, 81, 066201
Sanders, R. H. 2003, MNRAS, 342, 901
Simon, J. D. 2019, ARA&A, 57, 375
Tiret, O., & Combes, F. 2007, A&A, 464, 517
Trippe, S. 2014, ZNatA, 69, 173
Umetsu, K. 2020, A&ARv, 28, 7
Weinberg, M. D., & Katz, N. 2002, ApJ, 580, 627
Will, C. M. 2014, LRR, 17, 4
Yennapureddy, M. K., & Melia, F. 2018, PDU, 20, 65